High-resolution measurements and simulation of stratospheric and tropospheric intrusions in the vicinity of the polar jet stream

Jürgen Beuermann,[1] Paul Konopka,[1] Dominik Brunner,[2] Oliver Bujok,[1,3] Gebhard Günther,[1] Daniel S. McKenna,[1,4] Jos Lelieveld,[5] Rolf Müller,[1] and Cornelius Schiller[1]

Received 1 October 2001; revised 4 March 2002; accepted 12 March 2002; published 21 June 2002.

[1] Pronounced filamentation of tropospheric and stratospheric air masses was observed on a flight in the vicinity of the polar jet stream during the STREAM 1998 campaign in Timmins, Canada. High-spatial resolution ozone and water vapor measurements showed highly variable structures for the investigated region. Reconstructing high-resolution potential vorticity (PV) fields using the reverse-domain-filling (RDF) technique reproduce the in-situ ozone measurements qualitatively. Measurements and RDF results show the intrusion of stratospheric air penetrating deep into the troposphere. The observed intrusions occur on smaller horizontal scales than generally assumed for tropopause folding events. Moreover, fine-scale structures of tropospheric air masses being lifted up into the stratosphere could be reconstructed by the RDF technique using the tropospheric tracer specific humidity in addition to the more conventional calculations for the stratospheric tracer PV. *INDEX TERMS:* 0368 Atmospheric Composition and Structure: Troposphere—constituent transport and chemistry; 3362 Meteorology and Atmospheric Dynamics: Stratosphere/troposphere interactions

1. Introduction

[2] Stratosphere-Troposphere Exchange (STE) is relevant for chemical, dynamical, and radiative processes occurring in the atmosphere. Here we focus on STE in the region of the mid-latitude upper troposphere/lowermost stratosphere (UT/LS) [e.g. *Fischer et al.*, 2002]. Tropopause deformations [*Reiter*, 1975] like tropopause folds and cut-off-lows can lead to the formation of tropospheric or stratospheric filaments. The latter, the so-called stratospheric streamers, were simulated by *Appenzeller et al.* [1996]. Appenzeller used the contour advection technique to create sub-synoptic scale tracer fields not present in meteorological analyses for the comparison with METEOSAT water vapor images. *Sutton et al.* [1994] showed the skill of the reverse-domain-filling technique (RDF) as another trajectory-based technique for reconstructing sub-synoptic structures present in observational data. Here, we use the RDF technique for the interpretation of filamentary structures indicated by high-spatial resolution in-situ tracer measurements obtained on a flight on July 15, 1998 during the STREAM (Stratosphere-TRoposphere Experiments by Aircraft Measurements) 1998 Summer campaign [*Fischer et al.*, 2002] in the mid-latitude UT/LS region.

2. Meteorology and In-Situ Observations

[3] The temporal evolution of the synoptic situation in the region investigated by the flight on July 15, 1998 can be depicted from Figures 1a–1c by a time sequence of isentropic potential vorticity (PV) maps on the 330 K potential temperature surface. These data are interpolated from ECMWF analysis on 14 isobaric surfaces with a vertical resolution of approximately 100 hPa near the tropopause and a horizontal resolution of $1° \times 1°$. On July 14, 06:00 UTC a region of stratospheric air characterized by PV values greater than 2 PVU (PVU = 10^{-6} Km^2 kg^{-1} s^{-1}) was located over the western coast of Canada, from which an elongated streamer (marked as 1) propagated eastwards (see Figures 1a and 1b). At the same time a trough (marked as 2) of cold polar, stratospheric air developed and was transported into the mid-latitudes. Towards July 16, 00:00 UTC the two stratospheric air masses 1 and 2 were advected to the region of the Hudson Bay and spun up cyclonically around each other leading to the formation of an anchor-shaped structure in the vicinity of the polar jet stream.

[4] The flight path for the flight on July 15, 1998 from Timmins, Canada, was planned accordingly to ECMWF forecasts and GOES water vapor images. The flight was conducted in dry and almost cloud free air [*Fischer et al.*, 2002] with the outward flight leg at the altitude of 7.8 km in north-westerly direction and the return leg at 9.8 km. The locations of the air parcels at 00:00 UTC on July 16 encountered along the flight path are estimated from forward and backward-trajectory calculations and are marked as a black line in Figure 1c.

[5] The payload of the Cessna Citation during the STREAM campaign consisted of several in-situ instruments measuring the trace gas composition (e.g. O_3, H_2O, CO, CO_2, CFCs, N_2O, NO) and aerosol particle distribution [*Fischer et al.*, 2002]. In the following, data from two instruments, both with temporal resolutions of one second (1 Hz, given the aircraft velocity: spatial resolution ≈150 m), are analyzed: an ozone chemiluminescence monitor [*Bregman et al.*, 1995] and a Lyman-α-Hygrometer measuring total water [*Zöger et al.*, 1999]. Potential temperature was derived from the on board temperature and pressure sensors. The time series for the flight showed strong variations for O_3 and H_2O mixing ratios (Figure 2). Similar variabilities are also present in other data sets e.g. those of CO and NO [H. Fischer, private communication, 1998]. The observed strong gradients (grey shaded areas in Figure 2) are not evident in the analyzed potential vorticity (aPV) and analyzed specific humidity (aSH) data interpolated from the ECMWF fields on the flight track.

3. Results From RDF Studies

[6] The reverse-domain-filling technique [*Sutton et al.*, 1994] is based on backward-trajectories for air parcels initialized on uniformly gridded (isentropic) surfaces. Trajectories are calculated backwards in time. For the time in the past PV is mapped to the parcel locations, using meteorological fields interpolated on isentropic surfaces. Assuming PV conservation along the trajectories, the mapped values for a certain trajectory length (TL) are moved forward to the initialized parcel positions, thus creating a high-resolution field for the time where observational data are available. The chosen (backward-)trajectory length, is no universal parameter. On the one hand a long TL is desirable since more time is available for the PV distribution to collapse to smaller scales. On

[1]Forschungszentrum Jülich GmbH, ICG-I, Jülich, Germany.
[2]ETHZ, Institute for Atmospheric Science, Zürich, Switzerland.
[3]Now at Verein Deutscher Ingenieure, Düsseldorf, Germany.
[4]Now at NCAR, ACD, Boulder, CO, USA.
[5]Max-Planck Institute für Chemie, Mainz, Germany.

0094-8276/02/2001GL014162

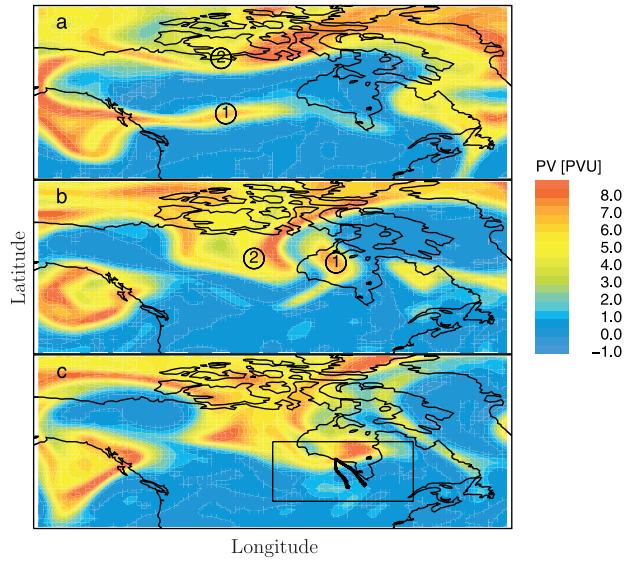

Figure 1. Analyzed potential vorticity (ECMWF) on the 330 K surface: (a) July 14, 1998, 06:00 UTC, (b) July 15, 1998, 06:00 UTC and (c) July 16, 1998, 00:00 UTC. The black line denotes the flight path transformed to the synoptic time July 16, 1998, 00:00 UTC by the use of forward and backward-trajectories.

the other hand the chosen TL is limited [*Sutton et al.*, 1994] i) by mixing processes driven by the dynamical properties of the flow (e.g. horizontal deformation, vertical stability) and ii) by increasing numerical errors for the trajectory calculations.

[7] For this case study isentropic backward-trajectory calculations were performed for air parcels initialized on uniformly gridded isentropic surfaces (horizontal spacing 0.1° × 0.1°), and vertical cross sections (horizontal spacing 60 s ≈ 9 km, vertical spacing 1 K) as well as for the positions of the flight track (spacing 1 s ≈ 0.15 km). For the RDF calculations based on ECMWF wind fields a scheme from R. Swinbank [*Sutton et al.*, 1994] and a slightly modified version [*McKenna et al.*, 1989] for the trajectory calculations along the flight track are used. In comparison to other case studies RDF calculations reconstructing not only the stratospheric tracer PV but also the tropospheric tracer specific humidity (SH) were conducted assuming the conservation of SH. Reconstructed PV (rPV) and SH (rSH) should be correlated with in-situ ozone and water vapor measurements, respectively.

[8] The upper panel of Figure 3 displays PV for a sub-area of Figure 1 (black frame in panel c) on the 332 K potential temperature surface. The aPV field shows the anchor-shaped structure of stratospheric air over the Hudson Bay, that is reflected in the in-situ data by the large ozone peak (at 00:20 UTC in Figure 2b). But, as mentioned above, the meso-scale trace gas variabilities observed along the flight path, indicated by the black boxes in Figure 3, are not present in the aPV field. For the RDF trajectory calculations, however, the rPV distribution in the region of the anchor-shape structure (Figure 3b, TL = 30 hours) shows interleaved stratospheric and tropospheric air masses. Moreover RDF reconstructs meso-scale structures of stratospheric air in the rPV pattern along the synoptic Cessna flight (black boxes in Figure 3 coincide with the grey marked stratospheric air masses 1 and 2 in Figure 2). A longer trajectory length of 60 hours produces more pronounced fine-scale filaments with larger gradients (Figure 3c).

[9] To investigate the three-dimensional structure of the observed situation we show vertical cross sections of PV and SH along the synoptic flight path in Figures 4a–4c and 4d–4f, respectively (more precisely: a vertical curtain containing the synoptic flight track). The cross section of aPV (Figure 4a) with small PV variations in the troposphere indicates a well-defined and uniform tropopause, denoted as dotted 2-PVU-isoline. The synoptic

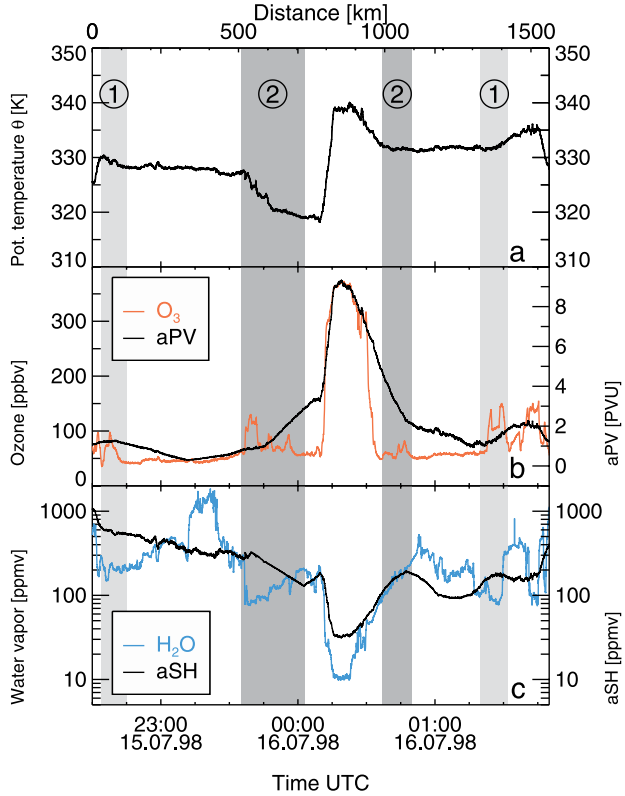

Figure 2. Time series for the flight on July 15, 1998. (a) Potential temperature (b) in-situ ozone (red line) and analyzed PV (from ECMWF, black line), (c) in-situ total water (blue line) and analyzed SH (from ECMWF, converted to ppmv, black line). Grey shaded areas mark four time ranges (on constant pressure levels) in regions 1 and 2 where strong tracer gradients were observed.

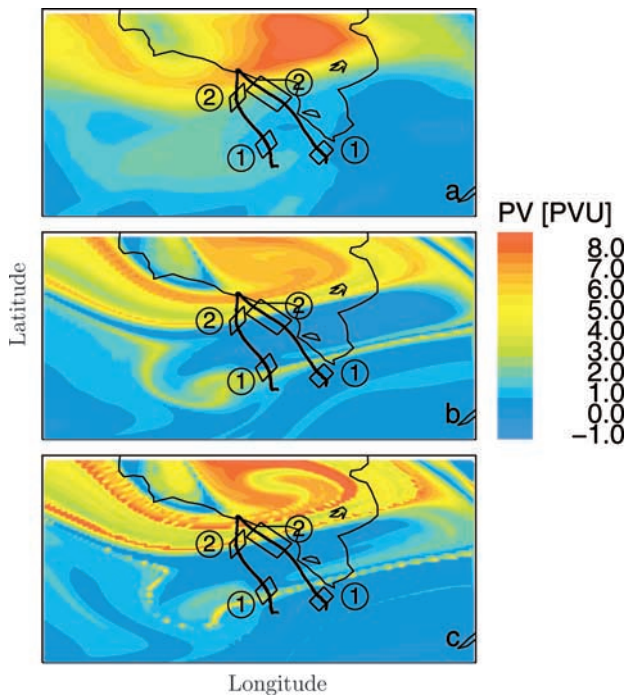

Figure 3. Isentropic maps of analyzed and reconstructed potential vorticity on the 332 K surface: (a) aPV (from ECMWF), (b) rPV for a TL of 30 hours, (c) rPV for a TL of 60 hours. The black boxes mark regions with strong gradients in the in-situ measurements (see Figure 2).

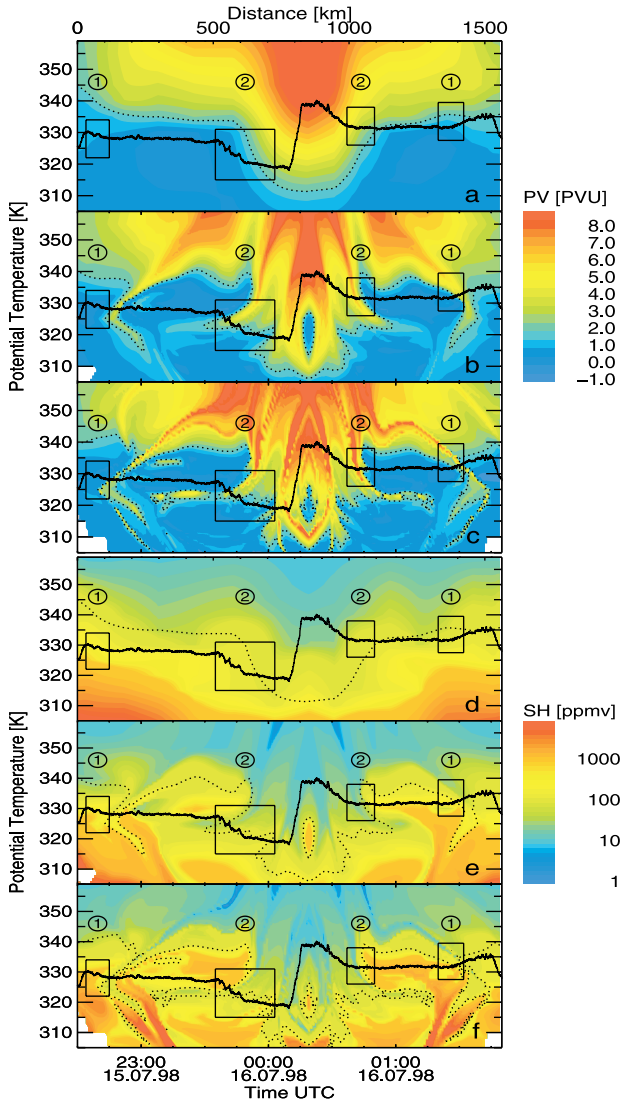

Figure 4. PV and SH (converted to ppmv, logarithmic color scale!) fields on a vertical cross section along the flight path (black solid line) with the 2-PVU-tropopause (dotted line): (a) aPV (from ECMWF), (b) rPV for a TL of 30 hours, (c) rPV for a TL of 60 hours, (d) analyzed SH (from ECMWF), (e) rSH for a TL of 30 hours, (f) rSH for a TL of 60 hours.

flight path of the Cessna (solid black line) transects the tropopause where the large ozone-peak occurs (00:20 UTC). The increased ozone values at this point correspond to the strong increase of PV when entering the stratosphere. The gradient of SH has opposite characteristics: low stratospheric SH values and increased, highly variable SH in the troposphere. At the time where the flight path crosses the tropopause and enters the stratosphere the cross section of aSH (Figure 4d, logarithmic color scale!) show low values that correspond to the minimum of the FISH water vapor data (Figure 2c). As for the isentropic maps the RDF calculations reconstruct sub-synoptic structures in the vertical rPV distributions (Figures 4b and 4c) showing interleaved stratospheric and tropospheric air masses around 00:20 UTC (i.e. in the anchor shaped structure). Additionally, meso-scale intrusions of stratospheric air into the troposphere occur for both employed TLs (30 and 60 h). These features, characterized by filaments with PV values greater than 2 PVU, correspond to the regions where in-situ variations of ozone are observed (black boxed areas). The coherent stratospheric intrusions reach down to 315 and 310 K for trajectory lengths of 30 and 60 hours, respectively. Vertical RDF cross sections of SH (Figures 4e and 4f) likewise reveal these intrusions. In addition to the rPV distributions, high rSH values between the stratospheric intrusions 1 and 2 demonstrate that also uplift of tropospheric air occurs. These tropospheric intrusions are correlated with the strong variations of in-situ water vapor data (see Figure 2c). The horizontal extent of the uplifted air is much larger compared to the observed stratospheric structures and reaches up to $\approx$ 350 K.

[10] Figures 5a and 5b display the ozone time series together with the rPV results along the (non-synoptic) flight path. The time series for a TL of 30 h shows the improvement over the aPV (Figure 2b) in resolving the stratospheric intrusions 1 and 2. A TL of 60 h leads to the formation of excessive rPV fine-scale variations, not present in the ozone measurements. For both TLs the stratospheric intrusions are slightly displaced. The time series of aSH matches only the general behavior of the water vapor data (Figure 2c, logarithmic scale!). In particular, the low water vapor mixing ratios ($\sim$10 ppmv) during the climb into the stratosphere (around 00:20 UTC), and the larger fluctuations in the troposphere between the stratospheric intrusions 1 and 2 reaching up to several hundred ppmv H_2O, are not reproduced. The analogous rSH time series (TL = 30 h, Figure 5d) gives a better reproduction of the in-situ data with lower mixing ratios for the climb and larger gradients for the region where intrusions of tropospheric air are observed (i.e. 23:10 to 23:30 UTC). A longer TL (TL = 60 h, Figure 5d) leads to the formation of fine-scale variations with extreme gradients of rSH (for the stratospheric intrusions) that are not present in the in-situ measurements.

4. Discussion

[11] The best qualitative correspondence between RDF results and observations was found for a TL of 30 h. Nonetheless, the

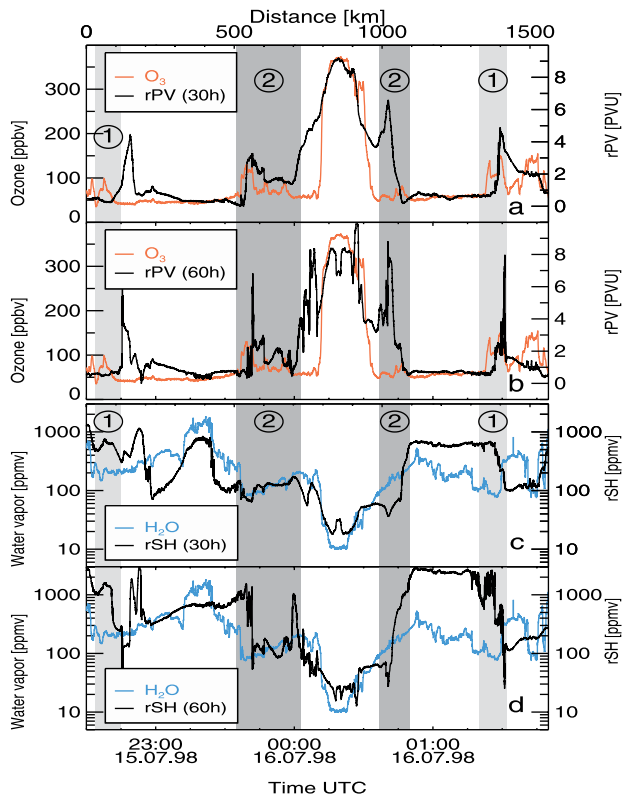

Figure 5. Time series of ozone and water vapor in comparison with reconstructed PV and SH (converted to ppmv, logarithmic scale!) for flight on July 15, 1998. (a) rPV for a TL of 30 hours, (b) rPV for a TL of 60 hours, (c) rSH for a TL of 30 hours, (d) rSH for a TL of 30 hours. Grey shaded areas as in Figure 2.

RDF calculations show some deficiencies in reproducing the observations quantitatively. Given the short time-scales considered numerical errors in the trajectory calculation are expected to be negligible. The main reason for errors in the absolute position of the observed structures in the RDF results (e.g. Figure 5) is most likely imperfect advection caused by small errors and the limited spatial and temporal resolution of the meteorological input fields. Further, deviations of the RDF results from the in-situ observations with respect to the strength of tracer gradients and the intensity of filamentation of the reconstructed fields are caused by the approximations and assumptions implied in the RDF technique. One assumption is tracer conservation within an air parcel along the trajectory path. However, in the real atmosphere mixing processes will reduce tracer gradients. Therefore, reconstructed parameters can only be in good agreement with observations whenever the influence of mixing processes is small. Further, in a strict sense different TLs should be used for individual trajectories since the intensity of mixing differs significantly for each air parcel depending on the deformation experienced during its advection history. Dehydration processes by condensation and subsequent particle sedimentation have an additional effect on the non-conservation of rSH as do rehydration processes explaining greater deviations for this parameter. Indeed, studies of ice saturation along the air parcel history and of the observed O_3/H_2O relation indicate that ice particles had formed in the air mass observed at ≈0:30 UTC on July 16, 1998 [*Khosrawi*, 2001]. Finally, the quality of the initial parameter fields influences the results obtained with RDF. Errors in the initial SH fields are particularly problematic [*Ovarlez et al.*, 2000] owing to the extreme SH gradients in the tropopause region.

[12] We investigated the validity of the assumption of isentropic transport. Heating rates calculated using the *Mocrette* [1991] scheme (no clouds) amount to $d\Theta/dt$ 1–3 K. Further, the influence of cross isentropic transport due the release of latent heat is likely to be small owing to the small amount of H_2O available for condensation in the upper troposphere and in particular in the lower stratosphere. Radiative cooling in the upper troposphere close to cloud decks can exceed 10 K for brief periods of much less than a day. However, GOES-8 infrared satellite images [*Fischer et al.*, 2002] show no clouds in the region of dry polar air probed by the considered flight. Deviations from isentropic transport influence the RDF-reconstructed parameters. However, RDF calculations considering the above mentioned radiative cooling/heating rates show only minor changes for the values of rPV and rSH in the stratosphere. The combined effect from cross isentropic transport and mixing processes has much stronger impact on rSH than on rPV due to the extreme (absolute) humidity gradients in the tropopause region. This behavior is reflected in the time series (Figure 5) where rPV reproduces the O_3 measurements better than rSH reproduces the H_2O observations.

[13] In summary, it appears that the differences between the observed O_3 and simulated rPV time series are mainly caused by uncertainties in the cross isentropic transport and by neglecting mixing processes. For the rSH fields, neglecting dehydration seems to be more important than the impact of mixing.

5. Conclusions

[14] This case study demonstrates the advantages of the RDF method as a simple and efficient technique for qualitatively reconstructing and identifying sub-synoptic structures (e.g. in high-spatial-resolution airborne measurements) that are not captured by conventional meteorological analyses. In the past RDF calculations were predominantly performed for PV, reconstructing the gradients in measurements of tracers with stratospheric origin (e.g. O_3). The results of SH-RDF calculations presented here are a valuable extension to PV-RDF resolving also the tropospheric gradients for tracers with opposite i.e. tropospheric characteristics (e.g. H_2O).

[15] The RDF calculations, confirmed by high-resolution tracer measurements, show the existence of coherent sheet-like stratospheric intrusions in the vicinity of the polar jet stream. RDF calculations for vertical cross sections along the flight path are especially helpful in the interpretation of such structures. The observed intrusions are similar in depth and morphology to the tongue-like stratospheric intrusions during tropopause folding events [e.g. *Shapiro*, 1980] penetrating deeply into the troposphere (310–315 K ≈ 600–500 hPa). In contrast to folds having horizontal dimensions of several hundred kilometers (perpendicular to the axis of the jet stream) the observed features occur on much smaller scales having a width of 50–200 km. With respect to STE the question is whether the discussed stratospheric (tropospheric) intrusions are irreversibly mixed into the troposphere (stratosphere). From the enlargement of the surface area of the interface between the two air masses an enhanced potential for mixing processes must be expected. Therefore the sheet-like intrusions of stratospheric air into the troposphere as presented here provides in-situ evidence for a precursor process causing quasi-isentropic STE.

[16] **Acknowledgments.** This work was supported by the EC through the STREAM project (ENV4-CT97-0544). We are grateful to the STREAM community, especially to the crew of the Cessna Citation. Further we thank P. van Velthoven (KNMI) for access to the ECMWF data, N. Thomas for assistance with the trajectory calculations and H. Fischer for helpful discussions.

References

Appenzeller, C., H. C. Davies, and W. A. Norton, Fragmentation of stratospheric intrusions, *J. Geophys. Res.*, *101*, 1435–1456, 1996.

Bregman, A., et al., Aircraft measurements of O_3, HNO_3, and N_2O in the winter Arctic lower stratosphere during the Stratosphere-Troposphere Experiment by Aircraft Measurements (STREAM) 1, *J. Geophys. Res.*, *100*, 11,245–11,260, 1995.

Fischer, H., D. Brunner, G. W. Harris, P. Hoor, D. S. McKenna, J. Rudolph, H. A. Scheeren, P. Siegmund, H. Wernli, J. Williams, and S. Wong, Chemical signatures of upper tropospheric airmasses over central Canada during stream 1998 summer campaign, *J. Geophys. Res.*, 2002, accepted.

Khosrawi, F., Modellierung der Bildung und des Wachstums von H_2SO_4/H_2O Aerosolen in der Stratosphäre und oberen Troposphäre, Ph.D. Thesis, Universität Bonn, 2001.

McKenna, D. S., R. L. Jones, J. Austin, E. V. Browell, M. P. McCormick, A. J. Krueger, and K. R. Chan, Analyses based on the United Kingdom Meteorological Office global model, *J. Geophys. Res.*, *94*, 16,847–16,854, 1989.

Mocrette, J.-J., Radiation and cloud radiative properties in the European Center for Medium range Weather Forecasts forecasting system, *J. Geophys. Res.*, *96*, 9121–9132, 1991.

Ovarlez, J., P. van Velthoven, G. Sachse, S. Vay, H. Schlager, and H. Ovarlez, Comparison of water vapour measurements from POLINAT 2 with ECMWF analyses in high-humidity conditions, *J. Geophys. Res.*, *105*, 3737–3744, 2000.

Reiter, E. R., Stratospheric-tropospheric exchange processes, *Rev. Geophys. Space Phys.*, *13*, 459–474, 1975.

Shapiro, M. A., Turbulent mixing within tropopause folds as a mechanism for the exchange of chemical constituents between stratosphere and troposphere, *J. Atmos. Sci.*, *37*, 994–1004, 1980.

Sutton, R. T., H. Maclean, R. Swinbank, A. O'Neill, and F. W. Taylor, High-resolution stratospheric tracer fields estimated from satellite observations using Lagrangian trajectory calculations, *J. Atmos. Sci.*, *51*, 2995–3005, 1994.

Zöger, M., C. Schiller, and N. Eicke, Fast in situ hygrometers: A new family of balloonborne and airborne Lyman-α photofragment fluorescence hygrometers, *J. Geophys. Res.*, *104*, 1807–1816, 1999.

D. Brunner, ETH Hönggerberg HPP, CH-8093 Zürich, Switzerland.

J. Lelieveld, MPI für Chemie, P.O. Box 3060, 55020 Mainz, Germany.

J. Beuermann, P. Konopka, G. Günther, D. S. McKenna, R. Müller, and C. Schiller, ICG-I, Forschungszentrum Jülich, 52425 Jülich, Germany. (ro.mueller@fz-juelich.de; p.konopka@fz-juelich.de; c.schiller@fz-juelich.de)